Entropy **2014**, *16*, 4101-4120; doi:10.3390/e16074101

OPEN ACCESS

entropy

ISSN 1099-4300

www.mdpi.com/journal/entropy

Article

Can the Hexagonal Ice-like Model Render the Spectroscopic Fingerprints of Structured Water? Feedback from Quantum-Chemical Computations

Javier Segarra-Martí, Daniel Roca-Sanjuán and Manuela Merchán *

Instituto de Ciencia Molecular, Universitat de València, P.O. Box 22085, 46071, Valencia, Spain; E-Mails: Javier.Segarra@uv.es (J.S.-M.); Daniel.Roca@uv.es (D.R.-S.);

* Author to whom correspondence should be addressed; E-Mail: Manuela.Merchan@uv.es; Tel.: +34-96-354-3155; Fax: +34-96-354-3274.

Received: 2 June 2014; in revised form: 14 July 2014 / Accepted: 16 July 2014 / Published: 21 July 2014

Abstract: The spectroscopic features of the multilayer honeycomb model of structured water are analyzed on theoretical grounds, by using high-level *ab initio* quantum-chemical methodologies, through model systems built by two fused hexagons of water molecules: the monomeric system [$H_{19}O_{10}$], in different oxidation states (anionic and neutral species). The findings do not support anionic species as the origin of the spectroscopic fingerprints observed experimentally for structured water. In this context, hexameric anions can just be seen as a source of hydrated hydroxyl anions and cationic species. The results for the neutral dimer are, however, fully consistent with the experimental evidence related to both, absorption and fluorescence spectra. The neutral π-stacked dimer [$H_{38}O_{20}$] can be assigned as the main responsible for the recorded absorption and fluorescence spectra with computed band maxima at 271 nm (4.58 eV) and 441 nm (2.81 eV), respectively. The important role of triplet excited states is finally discussed. The most intense vertical triplet→triplet transition is predicted to be at 318 nm (3.90 eV).

Keywords: structured water; π-stacked water; excited states; theoretical spectroscopy; CASPT2

---

1. Introduction

The detailed understanding of interfacial water, as well as the specific role of solutes on it, has been during the last decade an area of increasing interest and active research [1–12]. A number of properties different from bulk water, such as viscosity, density, freezing temperature, relative permittivity, and distinct absorption and fluorescence spectra, have been characterized next to solid surfaces by different groups [2,8,10–12]. Thus, the wide body of accumulated experimental experience up to date seems to point out to the actual existence of water structuring. Structured (or ordered) water is observed adjacent to hydrophilic surfaces, a solute-free region, known for that reason as "exclusion zone" (EZ) [2,12,13]. Since structured water can be therefore seen as interfacial water, and most of the water in living organisms can be considered as interfacial, the name "liquid crystalline" has also been employed [14]. Consequently, "structured", "ordered", "EZ water", or "liquid crystalline" are indistinctly used in practice. Furthermore, experimental support has been recently given describing interfacial water as a "photonic crystal" [15]. Since the recent publication of the latest book produced by Pollack [12], one of the most active researchers in the field over the last decade, the term "fourth phase of water" to denote structured water is also becoming progressively popular. It is well-recognized by now that water is capable to shape and control biomolecules, a fundamental aspect in cell biology [16]. For instance, the right protein function lies ultimately in a proper balance between ordered and bulk water [17,18]. Whereas water inside of relaxed myofibrils is extensively hydrogen bonded, muscle contraction has been recently characterized by a loss of order in the muscle-protein complex, accompanied by a destructuring of hydration water [17].

The absorption spectrum with a band peaking at ~270 nm (~4.59 eV) has been revealed to be a unique characteristic of structured water in solutions of many different substances (salts, amino acids, sugars), similarly to the feature recorded in the EZ by using Nafion 117 solution/film [2]. All the fluorescence emissions for those same systems lay in the range 300–500 nm (4.13–2.48 eV), most of them in interval 400–490 nm (3.10–2.53 eV) [2]. Interestingly, a transition 270-nm phase, eventually leading to bulk water, has also been identified as ice melts [19]. On the contrary, the lowest-energy band of the absorption spectrum in the gas phase has a maximum at 7.447 eV [20], whereas the spectra of the liquid is dominated by a pronounced peak at about 8.2 eV, showing the absorption spectra of amorphous, hexagonal, and cubic ice a similar structure [21]. The different electronic spectra of water in the gas phase (formed by water molecules) with respect to liquid and solid water (composed by different water aggregates) reflects the distinct structural water motifs responsible for the recorded absorption in the respective phases. It is therefore expected that the basic geometry of structured water responsible for the observed peak at ~4.59 eV would also be different. The multilayer honeycomb ice-like model depicted in Figure 1, which has been recently proposed by Pollack and co-workers [12,19], seems to be consistent with the experimental evidence. It is worth recalling that water hexamers have been observed next to diverse surfaces, including metals [22,23], protein subunits [24], and graphene [25,26], as well as in supercooled water [27].

In the present contribution, the hexameric model for structured water is analyzed through the $H_{19}O_{10}$ monomer composed by two fused water hexagons (see Figure 1c). In order to better mimic the actual situation, both the anionic and the neutral systems of the monomer, involving 100 and 99 electrons, respectively, shall be considered.

Figure 1. (**a**) Schematic representation of the multilayer honeycomb ice-like model. (**b**) A ten-hexagon layer. (**c**) The $H_{19}O_{10}$ system composed by two fused water hexagons is the monomer used in the present theoretical study.

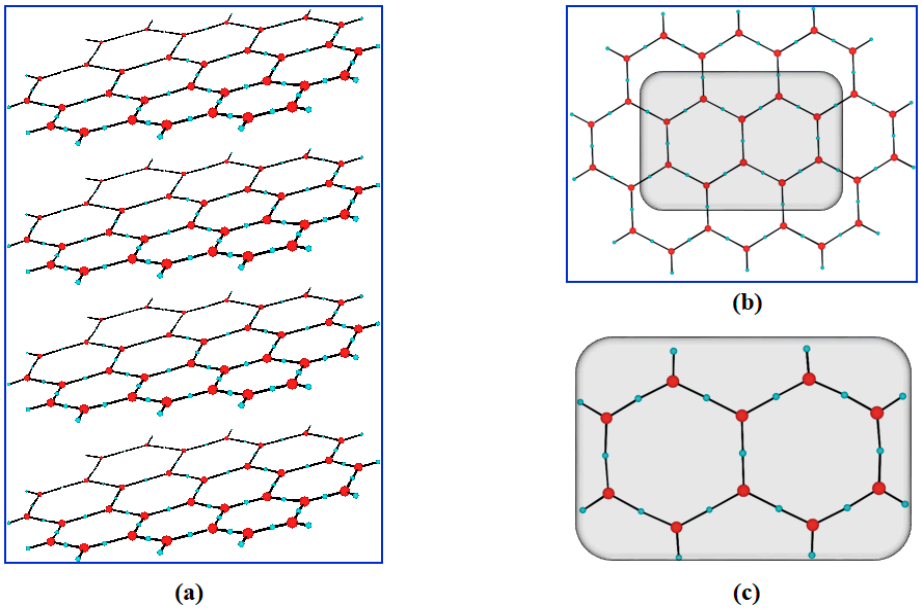

Based on our previous experience on the issue, where the relevance of π stacking has been highlighted [28,29], the corresponding π-stacked dimers [$H_{38}O_{20}$], comprising 200 and 198 electrons, would be subsequently considered. We pursue to get a satisfactory response on theoretical grounds to the following basic question: is the hexagonal ice-like model capable of rendering the spectroscopic fingerprints of structured water? For this purpose, high-level *ab initio* (from the first principles) quantum-chemical computations have been carried out in order to describe the relevant excited states and electronic transitions in the monomers (anion and neutral) and dimers (dianion and neutral) under study. In this manner, knowledge gathered on theoretical grounds may hopefully provide further insight into the water arrangements responsible for the spectroscopic features of structured water, which might be potentially relevant in the realms of biology, nanotechnology, and materials science.

2. Quantum Chemistry and Computational Strategies

The study has been performed within the framework of nonrelativistic Quantum Chemistry within the Born-Oppenheimer approximation [30]. Therefore, the electronic wave functions have been computed in the field of the bare nuclei. The electronic energy (E_{elec}), thus obtained, is added to the classical repulsion exerted by the nuclei (E_{rep}) leading to the total energy (E_{tot}). The latter describes the complex potential energy hypersurface of a given molecular system. It is precisely the delicate balance between E_{elec} (attractive) and E_{rep} (repulsive), which makes the bonding possible. As an illustrative example, the full configuration interaction (FCI) solution (exact solution within a given basis set) for the H_2 molecule employing a minimal STO-3G basis set, using the values for the molecular integrals from appendix D of [30], is shown in Figure 2. By a close inspection of the solutions around the equilibrium distance, as compared to the two isolated hydrogen atoms, one is able to conclude that the matrix elements related to the operator for the kinetic energy of the electrons and the Coulomb

attraction between electrons and nuclei are able to compensate the repulsion between the nuclei, 1/R in atomic units (a.u.), where R stands for the interatomic distance, as well as the repulsion between the electrons. Thus, the sum of the terms ascribed to an electron in the field of the nuclei (core Hamiltonian) can be seen as the main responsible of the binding interaction of the system, bringing a completely new quantum-mechanical view on the stability of the molecule. The possibility of sharing the two electrons in the same space around the two fixed nuclei makes possible the birth of a new species: the H_2 molecule. It is worth recalling at this point that the treatment of the spin of the electrons is within the nonrelativistic paradigm described phenomenologically. In short, the interaction between the nuclei is taken into account from a classic perspective, whereas the electronic energy is accounted for on the basis provided by Quantum Mechanics. Quantum Chemistry deals with the application of the basic quantum-mechanical principles to the study of atoms and molecules. The zero energy reference corresponds to an electron separated infinitely from a proton, that is, the energy of the proton is zero. The nature of the proton itself is therefore outside of the scope of standard Quantum Chemistry. At this resolution level, the proton is simply considered as a positive charge.

Figure 2. Potential energy curve of the H_2 molecule as a function of the bond length computed at the FCI/STO-3G level (see text). The energy (E) and the interatomic distance R(H-H) are given in atomic units (a.u.).

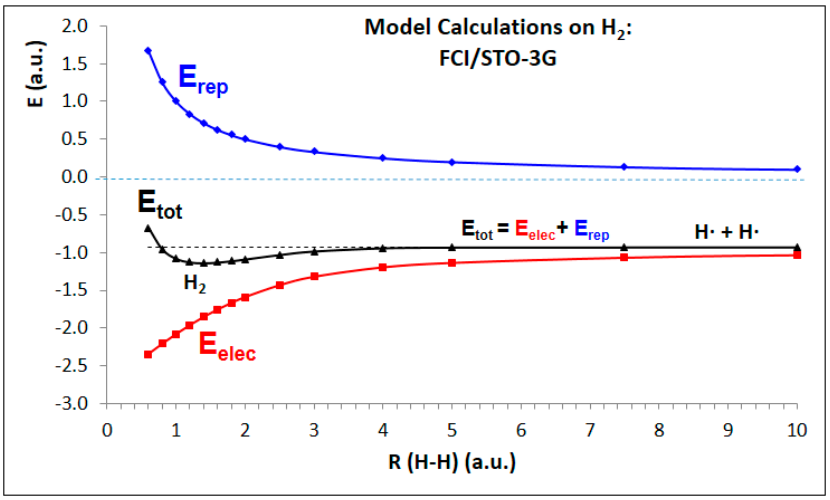

The major effort from a quantum-chemical standpoint is related, of course, to the correct description of the attractive potential E_{elec}, that is, the proper treatment of electron correlation. The movement of the electrons being correlated implies that the probability of finding two electrons at the same point in space becomes zero (the so-called Coulomb hole). Unfortunately, it is not the case for many approximate wave functions. Except for small molecular systems, exact solutions are not technically feasible. Therefore, one has to deal with truncated quantum-chemical algorithms, making special emphasis on the magnitude of the property of interest to be calculated, e.g., an electronic transition energy. The predicted value should become stable upon further improvements, reflecting so the balanced treatment performed in the electron correlation effects, both in the ground and excited states. In this sense, the CASPT2 (*Complete-Active-Space Second-Order Perturbation Theory*) method proposed by Roos and co-workers in the early nineties represented a fundamental breakthrough in *ab initio* computational work [31]. Electronic transitions could then be characterized on theoretical

grounds, within a few tenths of eV in practice, with respect to comparable experimental data in a variety of compounds of different molecular size, ranging from ethene to free-base porphyrin [32–37]. It represented quite an outstanding outcome two decades ago because error bars of about one eV used to be more a rule that an exception in previous *ab initio* research. We are quite confident by now in the predictive character of the CASPT2 methodology, which makes possible a suited analysis of experimental and theoretical work on an equal footing. Normally, the experimental-theoretical combined joint efforts produce a fruitful synergy favoring the deepest understanding of a given subject. The underlying reason clearly relies on the fact that we do not simulate but predict the intrinsic molecular properties of the treated compounds. Of course, the theoretical results are independent of any past, present, or future experimental work.

The CASPT2 method can be framed within single-reference second-order perturbation theory where a multiconfigurational CASSCF (*Complete Active Space Self-Consistent Field*) wave function is used as zeroth-order wave function. The zeroth-order Hamiltonian as originally implemented has been used [31] employing the MOLCAS-7 software package [38,39]. The CASSCF wave function is defined by the user, given by a number of active electrons and active orbitals based on the needs of the system according to the target to be achieved. The active electrons are distributed among the active orbitals in all possible ways consistent with the spatial and spin symmetry of the wave function required. Namely, the CAS space is of FCI type within the subspace spanned by the active orbitals and electrons. Both orbitals (one-electron functions) used to build the many-electron wave function (spin-adapted linear combination of determinants) and coefficients of the CASSCF expansion are optimized by means of the variation principle (search of stationary point). Details on the active spaces employed will be next given as appropriate. The oxygen 1s electrons have been kept frozen in the perturbation step. In order to minimize weakly interacting intruder states, the imaginary level-shift technique, with a value of 0.2 a.u., has been employed [40]. Ground-state geometry optimizations have been performed at the MP2 (*Second-Order Møller-Plesset Perturbation Theory*) level through the program GAUSSIAN 09 [41]. The basis set 6-31G** has been used throughout, as a compromise between accuracy and computational resources [32–37,42,43].

3. Results and Discussion

The results are presented in three subsections. Firstly, the vertical electronic absorption spectrum for the anionic system formed by two fused hexagons built by water molecules, that is, the $[H_{19}O_{10}]^-$ monomer, is considered. The structural evolution of the anionic dimer $[H_{38}O_{20}]^{2-}$ is then analyzed. Secondly, the absorption spectrum for the corresponding neutral species, the radical system $[H_{19}O_{10}]$ and its π-stacked dimer $[H_{38}O_{20}]$, is reviewed. For the π-stacked neutral dimer, the fate of the absorbed energy is subsequently explored and the results are related to the observed fluorescence features. Finally, the relevance of the triplet manifold is put forward and the most intense electronic transition of the triplet-triplet spectrum is predicted.

3.1. Anionic Systems

As originally proposed [12,44], the ice-like multilayer model of structured water is formed by a network of fused hexagon units (see Figure 1) negatively charged. Assuming that the charge

contribution made by each oxygen atom is minus two while that for each hydrogen atom is plus one, the net charge of the ten-hexagon structural diagram drawn in Figure 1b is −9. In general, for N-fused hexagons, the charge acquired by the global system is 1-N [44]. Therefore, from a molecular standpoint, the smallest model unit corresponds to the anionic monomer $[H_{19}O_{10}]^-$ bearing a negative charge −1. For each couple of fused hexagons built, a proton is assumed to be released. Thus, the model is particularly appealing because it accounts for the local charge separation between the EZ and the regions beyond observed by using pH measurements [45].

The main geometrical parameters for the ground-state equilibrium structure obtained for the $[H_{19}O_{10}]^-$ anionic system at the MP2/6-31G** level, together with the charge reorganization derived from Mulliken population analysis, are shown in Figure 3. Instead of two fused hexagons with bond-equalized O-H bond lengths, as it occurs for the ground state of the neutral species [29], the results for the anionic system can be seen as a reminiscent of a Zundel cation $H_5O_2^+$ in the middle of the system plus two anionic $H_3O_2^-$ species situated on the left- and right-side, those being hydrated by four nearly neutral water molecules (top and bottom). The trends described are maintained for layers formed by a larger number of fused hexagons. For instance, in the ten-hexagon system depicted in Figure 1b, specifically the $[H_{55}O_{32}]^{9-}$ anionic system, the structure of the two fused hexagons displayed in Figure 3 prevails in the center, which is surrounded by a number of hydrated hydroxyl anions. Thus, anions do not favor the formation of honeycomb-like layers but causes a pronounced charge polarization ending up in positively and negatively charged species. Among the latter, a clear contribution of hydroxyl anions is noted.

The vertical electronic transitions for the $[H_{19}O_{10}]^-$ anionic system have been computed at the ground-state geometry. The selection of the active space has been based on the nature and distribution of the canonical orbitals in the closed-shell system. There is a clear gap in orbital energies between the HOMO–5 and HOMO–6 and the LUMO+5 and LUMO+6, where HOMO and LUMO stand for the highest occupied molecular orbital and the lowest unoccupied molecular orbital, respectively. Consequently, the MOs topologically equivalent to the highest six occupied canonical MOs and the lowest six unoccupied MOs have been employed. It corresponds to 12 electrons distributed in 12 active MOs, hereafter denoted as CASSCF(12,12). Specifically, the number of active orbitals employed belonging to the irreducible representations a_g, b_{3u}, b_{2u}, b_{1g}, b_{1u}, b_{2g}, b_{3g}, a_u, of the D_{2h} symmetry point group are 2, 1, 2, 1, 2, 2, 1, 1, respectively. In each symmetry, the lowest root at the CASSCF(12,12) level has been computed. For the sake of completeness, the inactive orbitals employed are also given: 11, 2, 10, 2, 9, 1, 8, 1. The core orbitals (3, 0, 3, 0, 2, 0, 2, 0) have been kept frozen at the second-order level. The corresponding results corrected up to second order shall be labeled as CASPT2(12,12).

Table 1 compiles the results for the vertical electronic transitions obtained at the CASPT2(12,12) level for the $[H_{19}O_{10}]^-$ anionic system, together with the associated oscillator strengths, and information on the nature of the electronic excited states in terms of the corresponding CASSCF(12,12) natural orbitals (NOs), which are shown in Figure 4. As expected, the ground state is well described by the single closed-shell Hartree-Fock (HF) type configuration with a weight in the CASSCF wave function of 98%. The computed excited states show however multiconfigurational character.

Figure 3. (**a**) Selected optimized geometrical parameters (in Å and degrees) for the 1^1A_g ground state of the $[H_{19}O_{10}]^-$ anionic system computed at the MP2/6-31G** level (D_{2h} symmetry). (**b**) Net group charges derived from Mulliken population analysis.

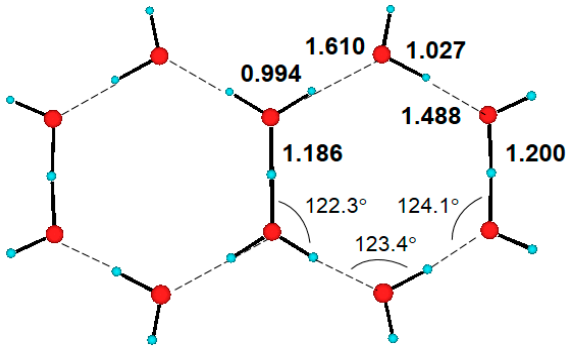

(a)

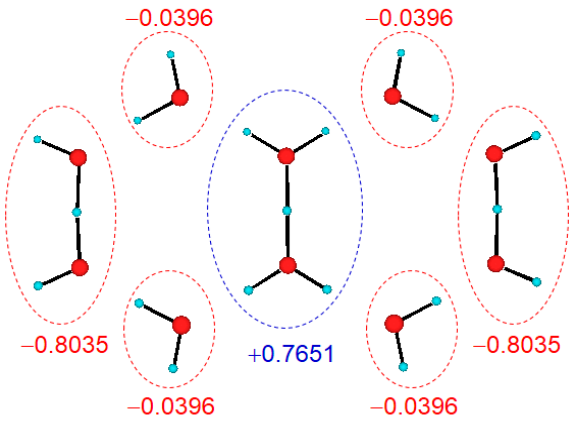

(b)

Table 1. Vertical transition energies (ΔE) and related oscillator strengths computed for the $[H_{19}O_{10}]^-$ anionic system at the CASPT2(12,12)/6-31G** level.

State	ΔE [eV]	ΔE [nm]	Oscillator strength	Assignment (Weight) [a]
1^1A_g (ground state)				closed-shell HF (98%)
1^1B_{1g}	7.42	167	forbidden	HOMO–2 → LUMO (46%) HOMO–3 → LUMO+1 (45%)
1^1A_u	7.42	167	forbidden	HOMO–3 → LUMO (46%) HOMO–2 → LUMO+1 (45%)
1^1B_{3g}	7.49	166	forbidden	HOMO → LUMO (51%) HOMO–1 → LUMO+1 (48%)
1^1B_{2u}	7.51	165	0.2431	HOMO–1 → LUMO (49%) HOMO → LUMO+1 (49%)
1^1B_{3u}	8.34	149	0.0382	HOMO–4 → LUMO (44%) HOMO–5 → LUMO+1 (42%)
1^1B_{2g}	8.34	149	forbidden	HOMO–5 → LUMO (43%) HOMO–4 → LUMO+1 (43%)

[a] Weight percentage of the given configuration in the CASSCF(12,12) wave function within parentheses.

The six electronic transitions obtained for the $[H_{19}O_{10}]^-$ anionic system can be grouped in three pairs of degenerate features centered at 7.4, 7.5, and 8.3 eV. For the monomer, the $[H_{19}O_{10}]^-$ anionic system, the lowest-lying excited states are energetically far away from that characteristic of structured water. The two lowest excited states 1^1B_{1g} and 1^1A_u, appearing at 7.42 eV (167 nm), are mainly described by a linear combination of one-electron promotions involving charge reorganization from the π system of the molecule towards the σ region. The states resemble to the lowest excited state of the water molecule itself, both in nature and energetic placement [46,47]. The corresponding vertical electronic transitions are forbidden. In increasing ordering of energy, the electronic states 1^1B_{3g} and 1^1B_{2u} of σ-σ* character are next found. The vertical electronic transition $1^1A_g \rightarrow 1^1B_{2u}$ placed at 7.51 eV (165 nm) has the largest oscillator strength with a computed value of about 0.24. The 1^1B_{2u} state is described by the linear combination of the configurations HOMO–1 → LUMO and HOMO → LUMO+1 with equal weights (49%). Finally, the 1^1B_{3u} and 1^1B_{2g} states of π-σ* nature are predicted at 8.34 eV (149 nm). The vertical transition from the ground state to the former has an oscillator strength of around 0.04.

Figure 4. Canonical orbitals and the respective orbital energies derived from a closed-shell Hartree-Fock computation obtained at the MP2/6-31G** optimized geometry of the ground-state 1^1A_g for the $[H_{19}O_{10}]^-$ anionic system. The related natural orbitals derived from the CASSCF(12,12) computation are also included The isodensity surface value for the orbitals is 0.030.

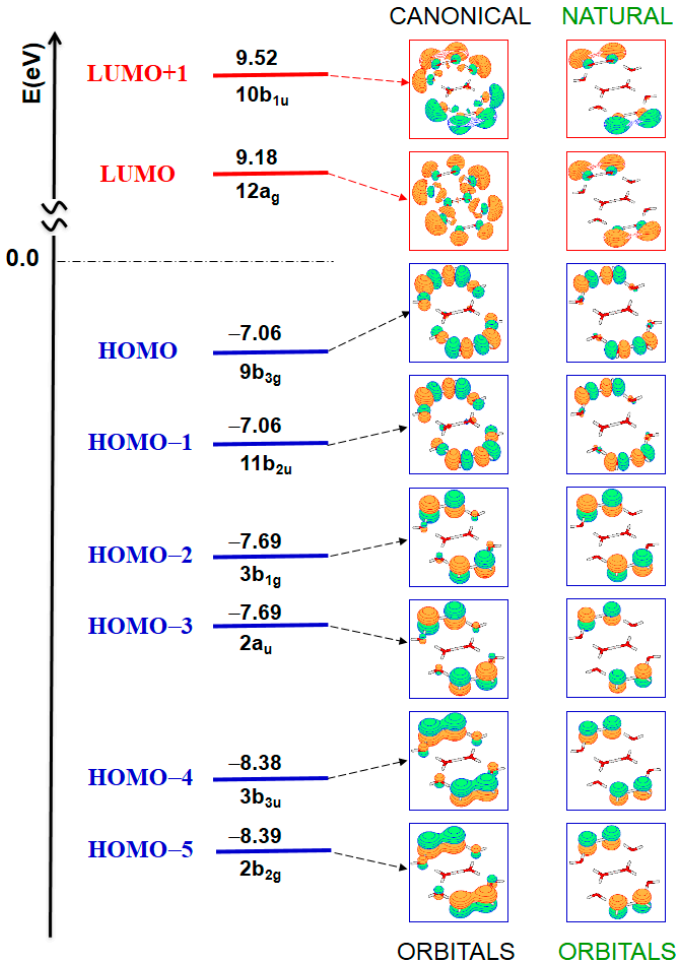

When two $[H_{19}O_{10}]^-$ anionic systems are situated in a parallel orientation at 2.4 Å within the constraints of D_{2h} symmetry (see Figure 5a), geometry optimization of the resulting global system $[H_{38}O_{20}]^{2-}$ leads, after a long optimization process where the original spatial symmetry is lost and breaking of the wave function occurs, to the bulk-type water aggregate displayed in Figure 5b.

Figure 5. (**a**) Input provided to the geometry optimization process of two layers formed by the anionic monomers $[H_{19}O_{10}]^-$. (**b**) Output obtained for the geometry optimization of dianion molecular system $[H_{38}O_{20}]^{2-}$ at the MP2/6-31G** level. White arrows are pointing to hydroxyl anions.

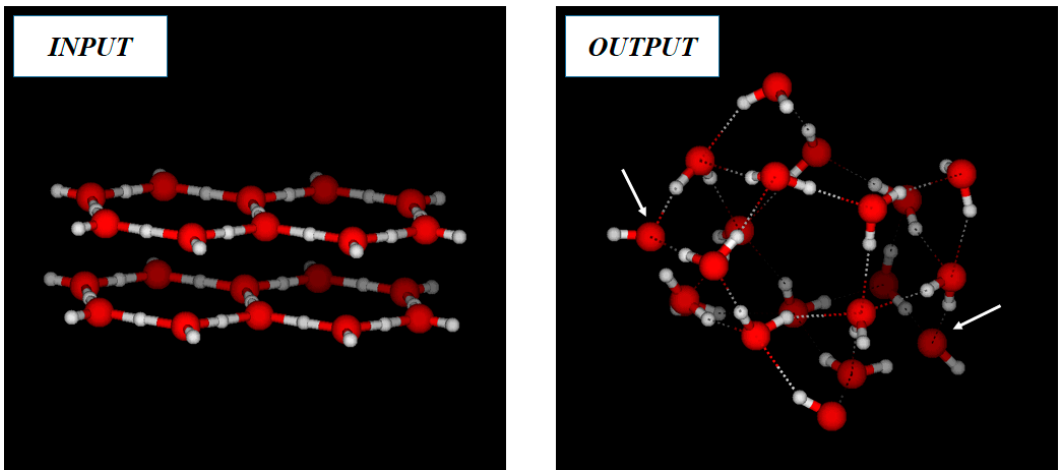

(a) (b)

According to the present results, a negatively charged monolayer formed by two fused water hexagons tends to produce hydrated hydroxyl anions and Zundel-like cations. Thus, in a layer, a negative charge is not equally spread over the entire system. Moreover, the findings do not support a stabilizing interaction activity between the different negatively charged layers (*cf.* Figure 5) as originally proposed for the hexagonal ice-like model [12,44]. The interaction of such anionic layers collapse towards the formation of hydrated hydroxyl anions in bulk-type structures, which are not expected to contribute to the absorption recorded at ~270 nm (4.59 eV) [2]. Therefore, they have not been considered further. For these reasons, in our quest to elucidate the basic molecular units responsible of the unique spectroscopic absorption of structured water, anionic species are discarded.

3.2. Neutral Systems

3.2.1. Absorption Spectroscopic Features

The vertical electronic spectra at the respective MP2/6-31G** geometries of the ground-state neutral monomer and dimer, the radical $[H_{19}O_{10}]$ and the π-stacked system $[H_{38}O_{20}]$, have been previously reported [29]. As stated above, in contrast to the optimized parameters for the ground-state anionic monomer, for the ground-state neutral monomer all the O-H bond distances are similar (around 1.2 Å, see Figure 6a). On the other hand, the interaction of two radical species leads to a stabilization of the dimer by more than 2 eV, characterized for a relatively short inter-monomer distance between the fused central oxygen atoms belonging to different monomers (2.115 Å, see Figure 6).

Figure 6. (**a**) MP2/6-31G** optimized parameters for the 1^2B_{2u} ground state of the neutral radical $[H_{19}O_{10}]$. The molecule is placed in the yz plane with the central O-H-O moiety along the y axis (D_{2h} symmetry). (**b**) Optimized parameters obtained for the 1^1A_g state of the π-stacked system $[H_{38}O_{20}]$ formed by two symmetrically oriented monomers (D_{2h} symmetry) at the MP2/6-31G** level. The R(O-O) value for the ground-state optimized structure is equal to 2.115 Å [29].

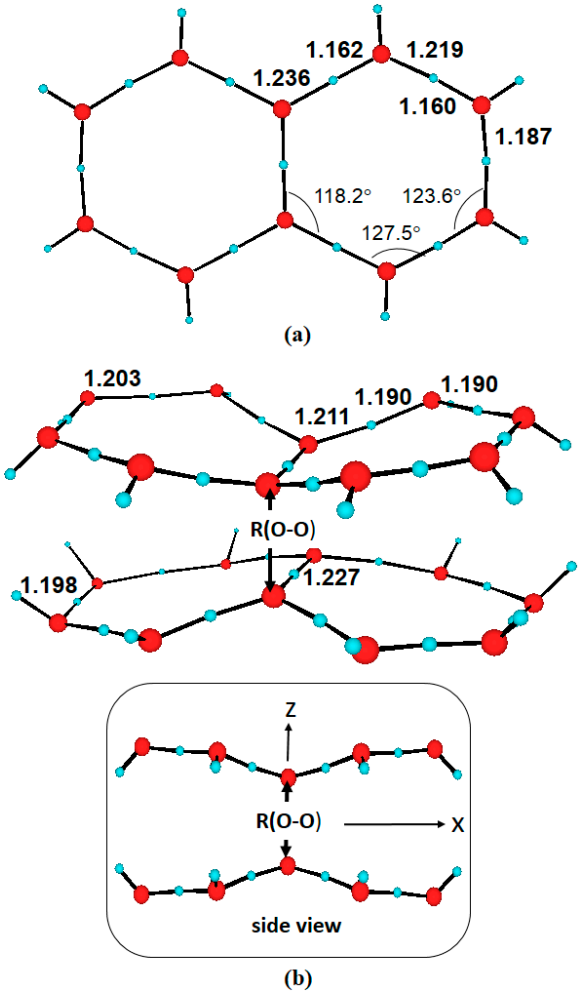

The radical monomer $[H_{19}O_{10}]$ certainly constitutes a versatile unit, having two spectroscopic features in the near infrared region (50,000–770 nm; 0.02–1.61 eV), two in the visible range (770–390 nm; 1.61–3.32 eV), and two in the near ultraviolet zone (390–200 nm; 3.22–6.62 eV). The six vertical electronic transitions found in the energy range up to 5 eV are shown in Figure 7. The doublet states are in all cases well described by the corresponding singly occupied natural orbital (SONO) of the CASSCF(13,12) wave function employed [29]. The vertical electronic transitions $1^2B_{2u} \rightarrow 1^2A_u$ and $1^2B_{2u} \rightarrow 1^2B_{2g}$ placed at 4.42 and 4.45 eV, respectively, are consistent with the spectroscopic signature of structured water with a maximum recorded at ~4.59 eV [2]. However, the dipole-forbidden nature of those features pushed us to keep searching for a more notorious molecular system that would become without any hesitation an excellent candidate of the 270-nm absorption determined experimentally [2]. As shall be discussed next, the π-stacked dimer $[H_{38}O_{20}]$ is able to fulfill such expectation.

Figure 7. Schematic representation of the six low-lying electronic transitions computed for the radical monomer [$H_{19}O_{10}$] at the CASPT2(13,12) level. The singly occupied natural orbitals (SONOs) derived from the CASSCF(13,12) wave function describing the respective states are also displayed [29].

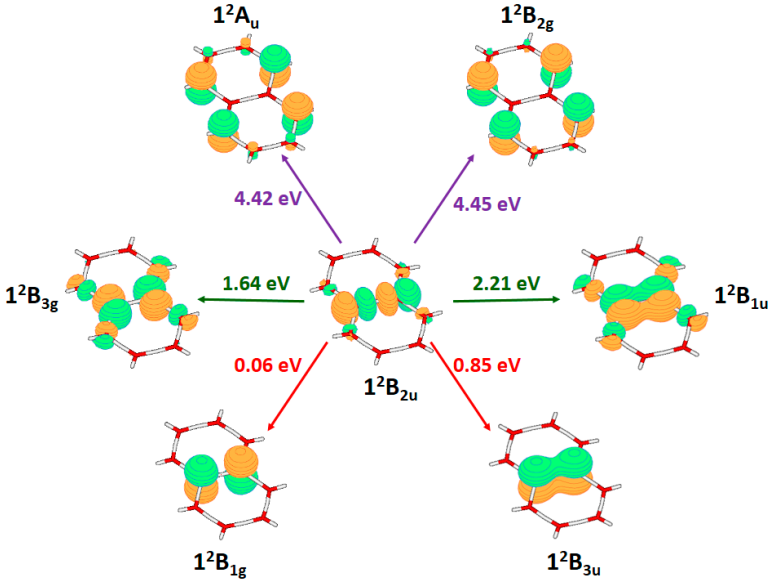

A total of twelve singlet→singlet electronic transitions have been computed for the [$H_{38}O_{20}$] system, seven in the visible range and five in the near ultraviolet region. In the latter, the electronic transition $1^1A_g \rightarrow 2^1B_{1u}$ of π character has been predicted at 4.58 eV (271 nm), with a computed oscillator strength of 0.29 [29], which perfectly matches with the experimental band maximum recorded at ~270 nm [2]. In terms of the natural orbitals (NOs) derived from the complex CASSCF(12,15) wave function employed [29], which corresponds to 12 electrons distributed among 15 active molecular orbitals, the electronic transition is depicted in Figure 8.

Figure 8. Schematic representation of the most intense transition $1^1A_g \rightarrow 2^1B_{1u}$ predicted for the π-stacked dimer [$H_{38}O_{20}$] at the CASPT2(12,15) level. The occupation numbers corresponding to the CASSCF(12,15) wave function for the NOs topologically equivalent to the HOMO-, LUMO-, and (HOMO–4)-like of the system are also included.

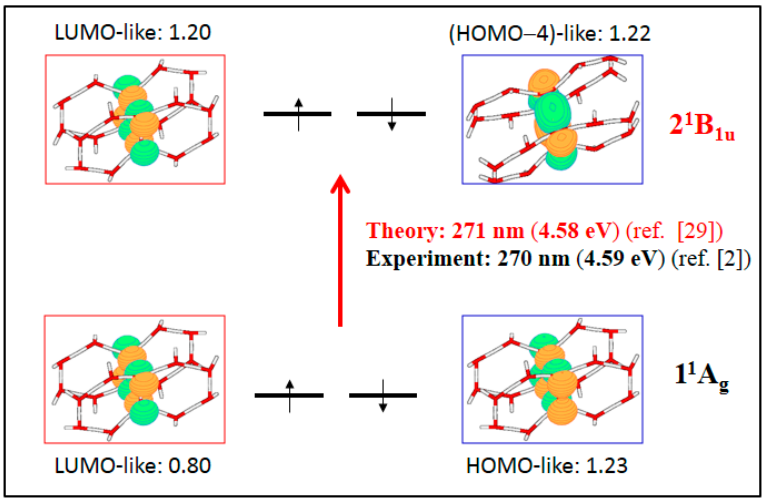

Based on the analysis of the occupation numbers of the active molecular orbitals in the respective CASSCF(12,15) wave functions, the ground state 1^1A_g (0.80 and 1.23) and the excited state 2^1B_{1u} (1.20 and 1.22) can be regarded as biradicals, the ground state having singly occupation numbers in the LUMO- and HOMO-like NOs and the brightest excited state in the LUMO- and (HOMO–4)-like NOs.

3.2.2. Fluorescence Spectroscopic Features

In order to determine the fate of the absorbed energy once the 2^1B_{1u} state has been populated, potential energy curves (PECs) with respect to the distance of the central fused oxygen atoms belonging to different monomers, R(O-O) in Figure 6, have been built for the twelve excited states, keeping the intra-monomer geometry fixed at that obtained for the ground state. In this manner, the effect of the variation of the inter-monomer distance, which can in principle be considered as the primary structural relaxation between the corresponding layers, can be analyzed. The most relevant results obtained from such comprehensive study are compiled in Figure 9. The results can be related to the fluorescence feature observed experimentally for many different kinds of compounds in the range 300–500 nm (4.13–2.48 eV), most of them in the interval 400–490 nm (3.10–2.53 eV) [2].

Figure 9. Potential energy curves for the main electronic states related to the absorption and fluorescence spectroscopic features of the π-stacked dimer [$H_{38}O_{20}$] built with respect to the inter-monomer distance R(O-O) (see Figure 6) obtained at the CASPT2(12,15) level in the present contribution.

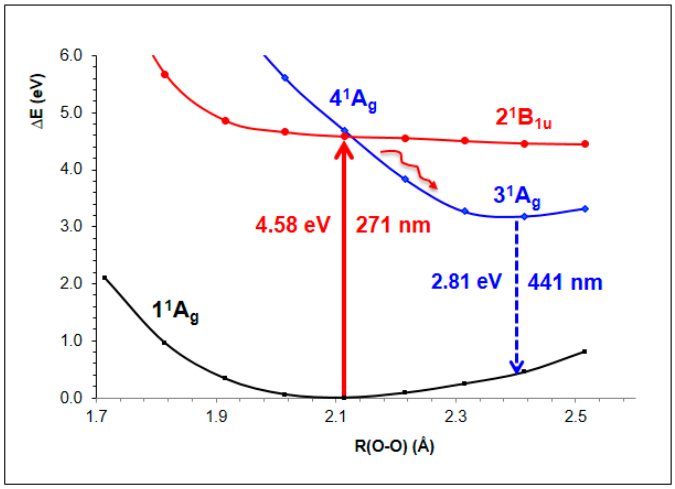

According to the relatively large oscillator strength calculated for the brightest $1^1A_g \rightarrow 2^1B_{1u}$ electronic transition [29], upon light absorption at the Franck-Condon (FC) region (around the ground-state equilibrium structure), the 2^1B_{1u} state is expected to be populated. The 2^1B_{1u} and 4^1A_g states computed vertically at 4.58 and 4.68 eV, respectively, are energetically close and can further interact. The PEC of the 2^1B_{1u} state has a flat character in an ample R(O-O) distance interval (2–2.6 Å). Conversely, the 4^1A_g state becomes relaxed adiabatically towards the minimum displayed in the 3^1A_g PEC placed at R(O-O) = 2.390 Å. Therefore, the occurrence of a crossing between the 2^1B_{1u} and 4^1A_g states in the vicinity of the FC region makes possible the transfer of population between the two hypersurfaces. From the minimum characterized for the 3^1A_g state, the system may then dissipate

energy by emitting radiation in the form of fluorescence. The predicted fluorescence peak is computed to be at 2.81 eV (441 nm), with an origin of band (T_e) of 3.20 eV (energy difference between the excited-state and ground-state minima). The results can be considered as upper bounds of the actual spectroscopic theoretical features (involving the full geometry optimization of the excited state). For the sake of completeness, let us recall that the 3^1A_g state, has a vertical excitation energy of 3.47 eV (357 nm) [29]. The PEC for the 2^1A_g state, as it also occurs for other low-lying excited states, is repulsive and it is not expected to be involved in the fluorescent process. The repulsive states lead to crossing regions with the ground state at large R(O-O) distances. The corresponding conical intersections may mediate in this way an effective nonradiative decay channel towards the repopulation of the ground state, as it occurs in DNA/RNA nucleobases [48–54]. The well found on the 3^1A_g hypersurface at 2.390 Å constitutes the only minimum accessible in the excited system. The fact that the nature of the excited state responsible for the absorption (2^1B_{1u}) and the fluorescence (3^1A_g) is different, nicely rationalizes the large Stokes shift observed experimentally [2]. The large difference between positions of the band maxima of the absorption and fluorescence spectra is then related to the different inter-monomer R(O-O) distance obtained for the ground state (2.115 Å) and the excited state (2.390 Å). The fluorescent state 3^1A_g at R(O-O) = 2.390 Å has a complex CASSCF(12,15) wave function with a marked multiconfigurational character dominated by the doubly excited configurations (HOMO-like)^2 → (LUMO-like)^2 (44%) and (HOMO–4) → (LUMO-like)^2 (26%), contributing also the closed-shell HF (13%), where the corresponding weights are reported within parentheses. The HOMO- and (HOMO–4)-like NOs have occupation numbers of 1.06, and 1.36, respectively. Thus, as can be seen schematically in Figure 10, the fluorescent state can also be considered approximately as a biradical.

Figure 10. Schematic representation of the fluorescent transition $3^1A_g \rightarrow 1^1A_g$ predicted for the π-stacked dimer [$H_{38}O_{20}$] at the CASPT2(12,15) level. The occupation numbers for the NOs topologically equivalent to the HOMO-, LUMO-, and (HOMO–4)-like for each state, corresponding to the CASSCF(12,15) wave function, are also included.

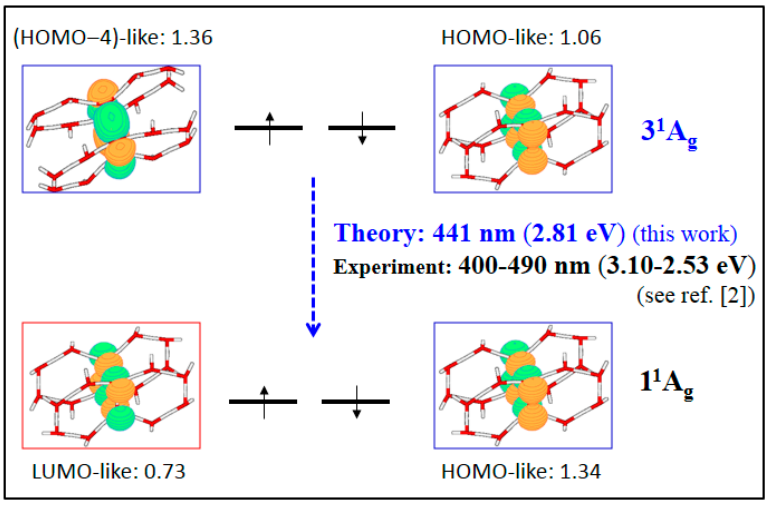

From an experimental standpoint, the wavelength of the emission peak (λ_{max}) depends on the wavelength of the excitation applied (λ_{exc}) in a variety of aqueous solutions employing different

solutes (salts, Nafion 117 solution/film, L-lysine, D-alanine, D-glucose, and sucrose) [2]. For instance, in the case of Nafion 117 solution, λ_{max} varies from 431 nm (2.88 eV) to 463 nm (2.68 eV), ranging λ_{exc} from 400–250 nm (3.10–4.96 eV). Moreover, the intensity increases when the λ_{exc} used is 270 nm (4.59 eV) or 250 nm (4.96 eV), peaking λ_{max} at 458–459 nm (2.71–2.70 eV) [2]. According to the present results depicted in Figure 9, at least 4.58–4.68 eV are required to reach the crossing region between the bright and the dark excited states, a process which ultimately causes the relaxation of the population towards the equilibrium region of the 3^1A_g hypersurface, from where the system may then emit light. The fluorescence feature computed here at 2.81 eV, which corresponds to the theoretical prediction for λ_{max}, is therefore consistent with the experimental findings [2].

3.2.3. On the Relevance of the Triplet Manifold

The importance of the triplet manifold becomes apparent taking into consideration the degeneracy computed between the lowest triplet state 1^3B_{2u} and the lowest singlet state 1^1A_g at the CASPT2(12,15) level. In other words, the ground state of the π-stacked dimer $[H_{38}O_{20}]$ can be equally described by the singlet state 1^1A_g and the triplet state 1^3B_{2u}. The latter, has as the leading configuration in the CASSCF(12,15) wave function the singly excited configuration HOMO-like→LUMO-like NOs (97% weight percentage). Therefore, a number of questions arise at this stage:

A. What is the "glue" that makes the singlet/triplet ground-state so stable?
B. What determines the population of the singlet or triplet ground state?
C. What about the most intense transition in the triplet manifold?

The understanding of the stability of the ground-state π-stacked dimer $[H_{38}O_{20}]$ relies on the same foundations as the description of the hydrogen molecule considered in Section 2. The high-level calculations performed at the CASPT2 level are in a large extent able to account for the attractive potential E_{elec}, characterizing correctly the system, which makes possible the balanced description of the intriguing π-stacked dimer through E_{tot}. Thus, the "glue" that enables the existence of the ground-state H_2 and the ground state of the $[H_{38}O_{20}]$ system in a seagull-like structure is the same: a purely quantum-mechanical effect able to describe properly the attractive potential of the electrons in the field of the nuclei, compensating the repulsive terms between the electrons and the nuclei.

The answer to question B will probably come from an interdisciplinary arena in the future. Just to remark on the importance of triplet states, it is worth recalling that they are especially sensitive to external forces such as electric and magnetic fields [55], which might be especially relevant in living organisms. Nanotechnological measurement of the electromagnetic activity of cells has been recently proposed in order to disclose the main features of pathological disturbances of coherent states in living organisms [56]. Moreover, information transfer without any transfer of matter (epitaxy), a well-documented and popularized technique in materials science can also be conceived as similar vectors [57].

The answer to question C is much easier to us and it also gives some clue to the issue put forward in B. The $1^3B_{2u}\rightarrow 2^3B_{3g}$ triplet→triplet vertical electronic transition is predicted at 3.90 eV (318 nm) at the CASPT2(12,15) level with an oscillator strength of 0.33. The 2^3B_{3g} state is described mainly by the doubly excited configuration (HOMO–3)-like, HOMO-like → (LUMO-like)^2 NOs (95% weight percentage). Thus, the feature is about 0.7 eV red shifted with respect to the main absorption found in

the singlet manifold at 4.58 eV (271 nm) [29]. Good tasting and clear uncontaminated water from a deep mountain has been reported to develop an absorption maximum in the range 290–310 nm (4.28–4.00 eV) [58]. On the other hand, it loses its capacity to absorb ultraviolet radiation in that range within a few days or weeks after being removed from groundwater, yielding so a criterion to the term "*fresh water*" [58]. As a reasonable working hypothesis, we tentatively assign the absorption feature of good mountain well water to the involvement of the most intense triplet→triplet electronic transition (see Figure 11).

Figure 11. Schematic representation of the most intense triplet→triplet vertical transition $1^3B_{2u} \rightarrow 2^3B_{3g}$ predicted for the π-stacked dimer [$H_{38}O_{20}$] at the CASPT2(12,15) level. The occupation numbers corresponding to the CASSCF(12,15) wave function for the NOs topologically equivalent to the HOMO-, LUMO-, and (HOMO–3)-like are also included.

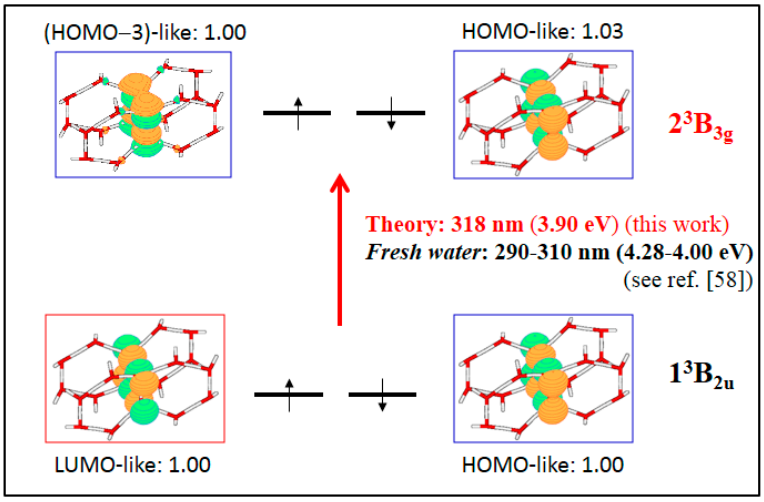

Ongoing work in our group is currently devoted to fully characterize the triplet manifold of the π-stacked dimer [$H_{38}O_{20}$], especially whether a possible phosphorescent state could contribute to the bluish color in the range of 450–490 nm (2.76–2.53 eV) ubiquitously encountered in pristine natural environments.

4. Conclusions

Within the framework of our own field of expertise in Theoretical and Computational Chemistry, on the basis of high level *ab initio* results, several conclusions can be drawn regarding the multilayer honeycomb model of structured water:

- For negatively charged multilayers, *i.e.*, anionic systems, the charge is not expected to be delocalized over the entire honeycomb layer. The system becomes polarized into hydrated hydroxyl anions and cationic moieties. Accordingly, the negative potential observed inside the EZ can be related to the presence of hydroxyl anions. The lowest-lying excited states found for the charged monolayer considered are about ~7.4 eV (~168 nm), well above the structured-water spectroscopic fingerprints determined experimentally ~4.59 (~270 nm). Therefore, we confidently conclude that heavily negatively charged hexagonally arrangements are not responsible for the observed spectroscopy.

- The spectroscopic features recorded for structured water are fully consistent with those computed for the neutral molecular models used to describe the essentials of the multilayer honeycomb arrangements. The neutral π-stacked dimer $[H_{38}O_{20}]$ has been revealed to be particularly suited for this purpose, both for the absorption and fluorescence events. The ground state of this unique system is equally well described by the 1^1A_g and 1^3B_{2u} states. Namely, the lowest singlet and the lowest triplet states show degeneracy. The relative large attractive interaction (more than 2 eV) between the two monomers $[H_{19}O_{10}]$ exerted by the (singlet/triplet) ground state of the dimer $[H_{38}O_{20}]$ can be related to the exclusion of many substances from the zone adjacent to various hydrophilic surfaces determined experimentally. The neutral π-stacked dimer $[H_{38}O_{20}]$ can be regarded as the main responsible for the recorded absorption with a computed band maximum at 271 nm (4.58 eV). On the other hand, the most intense vertical triplet→triplet transition is predicted to be at 318 nm (3.90 eV), which has been tentatively related to the absorption maximum observed in the range 290–310 nm (4.28–4.00 eV) for pristine water. The computed fluorescence features with band maximum at 441 nm (2.81 eV) is consistent with that registered experimentally in the range 400–490 nm (3.10–2.53 eV). In the singlet manifold, the absorbing bright excited state (2^1B_{1u}) and the fluorescent emitting state (3^1A_g) have distinct nature, which nicely rationalizes the large Stokes shift concomitant to the spectroscopy of structured water. The population transfer from the bright to the dark state occurs in the vicinity of the ground-state equilibrium structure (R(O-O) = 2.115 Å). The release of radiation as fluorescence can be accomplished by a slight separation of the two monomers in the π-stacked dimer $[H_{38}O_{20}]$ (R(O-O) = 2.390 Å).
- The underlying reason behind the successful description of the molecular systems considered is grounded on the ability of the CASPT2 method to treat in a balance manner the electron correlation effects of the electronic states in the different hypersurfaces explored. Despite the latter statement is supported up to date by more than two thousand calculations of excited states dealing with many different types of compounds, the fact is particularly outstanding in this case involving crystalline-like systems formed by hexagonally arranged water moieties, where a basic concept such as atomic valence becomes uncertain and quantum-mechanical effects able to describe the attractive potential properly have to be accounted for in a large extent.
- The research work presented emphasizes the quantization of matter at the molecular level, yielding the resonance conditions for the interaction with the electromagnetic radiation. Both aspects are complementary to describe the event actually taking place. Therefore, the results provided fully support the scenario envisioned in the realm of biology by Albert Szent-Györgyi. In the conclusion section of the book entitled "Bioenergetics" [59], published in 1957, he stated: *"Lucretian biochemistry involves the assumption that no interaction can take place between molecules without their touching one another. Support is given in this book to the idea that manifold interactions can take place without such bodily contact, either through energy bands or through the electromagnetic field, which thus appears with water and its structures as the matrix of biological reactions."*
  Quantum Chemistry shows indeed that water may form structures that absorb and transmit energy precisely in the same energy range as that arising from aromatic amino acids and DNA/RNA nucleobases.

Acknowledgments

The research reported has been supported by the Spanish MINECO project CTQ2010-14892 and the Juan de la Cierva programme (Ref. JCI-2012-13431).

Author Contributions

Calculations were mainly carried out by Javier Segarra-Martí. Daniel Roca-Sanjuán was primarily involved in the analysis and the discussions of the obtained findings. Manuela Merchán designed the current research project and took care of the writing of the paper. All authors have read and approved the final manuscript.

Conflicts of Interest

The authors declare no conflict of interest.

References and Notes

1. Ball, P. Water as an active constituent in cell biology. *Chem. Rev.* **2008**, *108*, 74–108.
2. Chai, B.H.; Zheng, J.M.; Zhao, Q.; Pollack, G.H. Spectroscopic studies of solutes in aqueous solution. *J. Phys. Chem. A* **2008**, *112*, 2242–2247.
3. Cheng, J.X.; Pautot, S.; Weitz, D.A.; Xie, X.S. Ordering of water molecules between phospholipid bilayers visualized by coherent anti-Stokes Raman scattering microscopy. *Proc. Natl. Acad. Sci. USA.* **2003**, *100*, 9826–9830.
4. Feng, I.; Kuo, W.; Mundy, C.J. An ab initio molecular dynamics study of the aqueous liquid-vapor interface. *Science* **2004**, *303*, 658–660.
5. Brown, G.E. How minerals react with water. *Science* **2001**, *294*, 67–69.
6. Ostroverkhov, V.; Waychunas, G.A.; Shen, Y.R. New information on water interfacial structure revealed by phase-sensitive surface spectroscopy. *Phys. Rev. Lett.* **2005**, *94*, 046102.
7. Jena, K.C.; Covert, P.A.; Hore, D.K. The Effect of Salt on the Water Structure at a Charged Solid Surface: Differentiating Second- and Third-order Nonlinear Contributions. *J. Phys. Chem. Lett.* **2011**, *2*, 1056–1061.
8. Yoo, H.; Paranji, R.; Pollack, G.H. Impact of Hydrophilic Surfaces on Interfacial Water Dynamics Probed with NMR Spectroscopy. *J. Phys. Chem. Lett.* **2011**, *2*, 532–536.
9. Chen, X.; Yang, T.; Kataoka, S.; Cremer, P.S. Specific ion effects on interfacial water structure near macromolecules. *J. Am. Chem. Soc.* **2007**, *129*, 12272–12279.
10. Tychinsky, V. High Electric Susceptibility is the Signature of Structured Water in Water-Containing Objects. *Water* **2011**, *3*, 95–99.
11. Bunkin, N.F.; Ignatiev, P.S.; Kozlov, V.A.; Shkirin, A.V.; Zakharov, S.D.; Zinchenko, A.A. Study of the Phase States of Water Close to Nafion Interface. *Water* **2013**, *4*, 129–154.
12. Pollack, G.H. *The Fourth Phase of Water: Beyond Solid, Liquid, and Vapor*; Ebner and Sons: Seattle, WA, USA, 2013.
13. Zheng, J.M.; Chin, W.C.; Khijniak, E.; Pollack, G.H. Surfaces and interfacial water: Evidence that hydrophilic surfaces have long-range impact. *Adv. Colloid Interface Sci.* **2006**, *127*, 19–27.

14. Ho, M.-W. *Living Rainbow H_2O*; World Scientific: Singapore, Singapore, 2012.
15. Bunkin, N.F.; Gorelik, V.S.; Kozlov, V.A.; Shkirin, A.V.; Suyazov, N.V. Colloidal Crystal Formation at the "Nafion-Water" Interface. *J. Phys. Chem. B* **2014**, *118*, 3372–3377.
16. Chaplin, M. Do We Underestimate the Importance of Water in Cell Biology? *Nat. Rev. Mol. Cell Biol.* **2006**, *7*, 861–866.
17. Yoo, H.; Nagornyak, E.; Das, R.; Wexler, A.D.; Pollack, G.H. Contraction-Induced Changes in Hydrogen Bonding of Muscle Hydration Water. *J. Phys. Chem. Lett.* **2014**, *5*, 947–952.
18. Schee, C.R.V.D.; Ooms, K.J. Investigating Water Interactions with Collagen Using ^{2}H Multiple Quantum Filtered NMR Spectroscopy To Provide Insights into the Source of Double Quantum Filtered Signal in Tissue. *J. Phys. Chem. B* **2014**, *118*, 3491–3497.
19. So, E.; Stahlberg, R.; Pollack, G.H. Exclusion zone as an intermediate between ice and water. In *Water and Society: Ecology and the Environment*; Jorgensen, S.E., Brebbia, A., Popov, V., Eds.; WIT: Southampton, UK, 2012; Volume 153, pp. 1–9.
20. Mota, R.; Parafita, R.; Giuliani, A.; Hubin-Franskin, M.J.; Lourenco, J.M.C.; Garcia, G.; Hoffmann, S.V.; Mason, N.J.; Ribeiro, P.A.; Raposo, M.; Limao-Vieira, P. Water VUV electronic state spectroscopy by synchrotron radiation. *Chem. Phys. Lett.* **2005**, *416*, 152–159.
21. Wernet, P.; Nordlund, D.; Bergmann, U.; Cavalleri, M.; Odelius, M.; Ogasawara, H.; Naslund, L.A.; Hirsch, T.K.; Ojamae, L.; Glatzel, P.; Pettersson, L.G.M.; Nilsson, A. The structure of the first coordination shell in liquid water. *Science* **2004**, *304*, 995–999.
22. Carrasco, J.; Santra, B.; Klimes, J.; Michaelides, A. To Wet or Not to Wet? Dispersion Forces Tip the Balance for Water Ice on Metals. *Phys. Rev. Lett.* **2011**, *106*, 026101.
23. Carrasco, J.; Hodgson, A.; Michaelides, A. A molecular perspective of water at metal interfaces. *Nat. Mater.* **2012**, *11*, 667–674.
24. McGeoch, J.E.M.; McGeoch, M.W. Entrapment of water by subunit c of ATP synthase. *J. R. Soc. Interface* **2008**, *5*, 311–318.
25. Cicero, G.; Grossman, J.C.; Schwegler, E.; Gygi, F.; Galli, G. Water Confined in Nanotubes and between Graphene Sheets: A First Principle Study. *J. Am. Chem. Soc.* **2008**, *130*, 1871–1878.
26. Kimmel, G.A.; Matthiesen, J.; Baer, M.; Mundy, C.J.; Petrik, N.G.; Smith, R.S.; Dohnálek, Z.; Kay, B.D. No Confinement Needed: Observation of a Metastable Hydrophobic Wetting Two-Layer Ice on Graphene. *J. Am. Chem. Soc.* **2009**, *131*, 12838–12844.
27. Michaelides, A.; Morgenstern, K. Ice nanoclusters at hydrophobic metal surfaces. *Nat. Mater.* **2007**, *6*, 597–601.
28. Segarra-Martí, J.; Coto, P.B.; Rubio, M.; Roca-Sanjuán, D.; Merchán, M. Towards the understanding at the molecular level of the structured-water absorption and fluorescence spectra: A fingerprint of π-stacked water. *Mol. Phys.* **2013**, *111*, 1308–1315.
29. Segarra-Martí, J.; Roca-Sanjuán, D.; Merchán, M. On the hexagonal ice-like model of structured water: Theoretical analysis of the low-lying excited states. *Comput. Theor. Chem.* **2014**, doi:10.1016/j.comptc.2014.02.012.
30. Szabo, A.; Ostlund, N.S. *Modern Quantum Chemistry: Introduction to Advanced Electronic Structure Theory*; Dover Publications: Mineola, NY, USA, 1996.
31. Andersson, K.; Malmqvist, P.-Å.; Roos, B.O. 2nd-Order Perturbation-Theory with a Complete Active Space Self-Consistent Field Reference Function. *J. Chem. Phys.* **1992**, *96*, 1218–1226.

32. Merchán, M.; Serrano-Andrés, L. Ab Initio Methods for Excited States. In *Computational Photochemistry*; Olivucci, M., Ed.; Elsevier: Amsterdam, The Netherlands, 2005; Volume 16, pp. 35–91.
33. Roca-Sanjuán, D.; Aquilante, F.; Lindh, R. Multiconfiguration second-order perturbation theory approach to strong electron correlation in chemistry and photochemistry. *Comput. Mol. Sci.* **2012**, *2*, 585–603.
34. Roos, B.O.; Andersson, K.; Fulscher, M.P.; Malmqvist, P.A.; Serrano-Andrés, L.; Pierloot, K.; Merchán, M. Multiconfigurational perturbation theory: Applications in electronic spectroscopy. *Adv. Chem. Phys.* **1996**, *93*, 219–331.
35. Serrano-Andrés, L.; Merchán, M. Quantum chemistry of the excited state: 2005 overview. *J. Mol. Struct.* **2005**, *729*, 99–108.
36. Merchán, M.; Serrano-Andrés, L.; Fülscher, M.P.; Roos, B.O. Multiconfigurational Perturbation Theory Applied to Excited States of Organic Molecules. In *Recent Advances in Multireference Theory*; Hirao, K., Ed.; World Scientific Publishing: Singapore, Singapore, 1999; Volume 4, pp. 161–195.
37. Serrano-Andrés, L.; Merchán, M. Spectroscopy: Applications. In *Encyclopedia of Computational Chemistry*; Schleyer, P.V.R., Ed.; Wiley: Chichester, UK, 2004.
38. Aquilante, F.; De Vico, L.; Ferré, N.; Ghigo, G.; Malmqvist, P.A.; Neograd y, P.; Pedersen, T.B.; Pitonak, M.; Reiher, M.; Roos, B.O.; Serrano-Andrés, L.; Urban, M.; Veryazov, V.; Lindh, R. Software News and Update MOLCAS 7: The Next Generation. *J. Comput. Chem.* **2010**, *31*, 224–247.
39. Aquilante, F.; Pedersen, T.B.; Veryazov, V.; Lindh, R. MOLCAS—a software for multiconfigurational quantum chemistry calculations. *Comput. Mol. Sci.* **2013**, *3*, 143–149.
40. Forsberg, N.; Malmqvist, P.-Å. Multiconfiguration perturbation theory with imaginary level shift. *Chem. Phys. Lett.* **1997**, *274*, 196–204.
41. Frisch, M.J.; Trucks, G.W.; Schlegel, H.B.; Scuseria, G.E.; Robb, M.A.; Cheeseman, J.R.; Scalmani, G.; Barone, V.; Mennucci, B.; Petersson, G.A.; Nakatsuji, H.; Caricato, M.; Li, X.; Hratchian, H.P.; Izmaylov, A.F.; Bloino, J.; Zheng, G.; Sonnenberg, J.L.; Hada, M.; Ehara, M.; Toyota, K.; Fukuda, R.; Hasegawa, J.; Ishida, M.; Nakajima, T.; Honda, Y.; Kitao, O.; Nakai, H.; Vreven, T.; Montgometry, J.A., Jr; Peralta, J.E.; Ogliaro, F.; Bearpark, M.; Heyd, J.J.; Brothers, E.; Kudin, K.N.; Staroverov, V.N.; Kobayashi, R.; Normand, J.; Raghavachari, K.; Rendell, A.; Burant, J.C.; Iyengar, S.S.; Tomasi, J.; Coss, M.; Rega, N.; Millam, J.M.; Klene, M.; Knox, J.E.; Cross, J.B.; Bakken, V.; Adamo, C.; Jaramillo, J.; Gomperts, R.; Stratmann, R.E.; Yazyev, O.; Austin, A.J.; Cammi, R.; Pomelli, C.; Ochterski, J.W.; Martin, R.L.; Morokuma, K.; Zakrzewski, V.G.; Voth, G.A.; Salvador, P.; Dannenberg, J.J.; Dapprich, S.; Daniels, A.D.; Farkas, O.; Foresman, J.B.; Ortiz, J.V.; Cioslowski, J.; Fox, D.J. *GAUSSIAN 09 Revision B.01*; Gaussian, Inc.: Wallingford, CT, USA, 2010.
42. Serrano-Andrés, L.; Merchán, M.; Borin, A.C. A Three-State Model for the Photophysics of Guanine. *J. Am. Chem. Soc.* **2008**, *130*, 2473–2484.
43. Serrano-Andrés, L.; Merchán, M.; Borin, A.C. Adenine and 2-Aminopurine: Paradigms of Modern Theoretical Photochemstry. *Proc. Natl. Acad. Sci. USA.* **2006**, *103*, 8691–8696.
44. Lippincott, E.R.; Stromberg, R.R.; Grant, W.H.; Cessac, G.L. Polywater. *Science* **1969**, *164*, 1482–1487.

45. Chai, B.H.; Yoo, H.; Pollack, G.H. Effect of Radiant Energy on Near-Surface Water. *J. Phys. Chem. B* **2009**, *113*, 13953–13958.
46. Rubio, M.; Serrano-Andrés, L.; Merchán, M. Excited states of the water molecule: Analysis of the valence and Rydberg character. *J. Chem. Phys.* **2008**, *128*, 104305.
47. Segarra-Martí, J.; Roca-Sanjuán, D.; Merchán, M.; Lindh, R. On the photophysics and photochemistry of the water dimer. . *J. Chem. Phys.* **2012**, *137*, 244309.
48. Olaso-González, G.; Roca-Sanjuán, D.; Serrano-Andrés, L.; Merchán, M. Toward the understanding of DNA fluorescence: The singlet excimer of cytosine. *J. Chem. Phys.* **2006**, *125*, doi:10.1063/1.2408411.
49. Roca-Sanjuán, D.; Olaso-González, G.; González-Ramírez, I.; Serrano-Andrés, L.; Merchán, M. Molecular basis of DNA photodimerization: Intrinsic production of cyclobutane cytosine dimers. *J. Am. Chem. Soc.* **2008**, *130*, 10768–10779.
50. González-Ramírez, I.; Climent, T.; Serrano-Pérez, J.J.; González-Luque, R.; Merchán, M.; Serrano-Andrés, L. The role of pyrimidine nucleobases excimers in DNA photoreactivity. *Pure Appl. Chem.* **2009**, *81*, 1695–1705.
51. Olaso-González, G.; Merchán, M.; Serrano-Andrés, L. The Role of Adenine Excimers in the Photophysics of Oligonucleotides. *J. Am. Chem. Soc.* **2009**, *131*, 4368–4377.
52. Climent, T.; González-Ramírez, I.; González-Luque, R.; Merchán, M.; Serrano-Andrés, L. Cyclobutane Pyrimidine Photodimerization of DNA/RNA Nucleobases in the Triplet State. *J. Phys. Chem. Lett.* **2010**, *1*, 2072–2076.
53. González-Ramírez, I.; Roca-Sanjuán, D.; Climent, T.; Serrano-Pérez, J.J.; Merchán, M.; Serrano-Andrés, L. On the photoproduction of DNA/RNA cyclobutane pyrimidine dimers. *Theor. Chem. Acc.* **2011**, *128*, 705–711.
54. Giussani, A.; Segarra-Martí, J.; Roca-Sanjuán, D.; Merchán, M. Excitation of Nucleobases from a Computational Perspective I: Reaction Paths. *Top. Curr. Chem.* **2013**, doi:10.1007/128_2013_501.
55. Lange, K.K.; Tellgren, E.I.; Hoffmann, M.R.; Helgaker, T. A Paramagnetic Bonding Mechanism for Diatomics in Strong Magnetic FIelds. *Science* **2012**, *337*, 327–331.
56. Pokorny, J.; Pokorny, J. Biophysical Pathology in Cancer Transformation. *J. Clin. Exp. Oncol.* **2013**, *S1*, 1–9.
57. Roy, R.; Tiller, W.A.; Hoover, M.R. The Structure of Liquid Water: Novel Insights from Materials Research. *Indian J. Res. Homeopath.* **2009**, *3*, 1–24.
58. DeMeo, J. Water as a Resonant Medium for Unusual External Environmental Factors. *Water* **2011**, *3*, 1–47.
59. Szent-Györgyi, A. *Bioenergetics*; Academic Press: New York, NY, USA, 1957.